mathematics

MDPI

Article

Linking Self-Organization of Bacterial and Human Populations in Mathematical Models of Chemotaxis

Romas Baronas [1,*], Boleslovas Dapkūnas [1] and Remigijus Šimkus [2]

[1] Institute of Computer Science, Faculty of Mathematics and Informatics, Vilnius University, Didlaukio 47, LT-08303 Vilnius, Lithuania; boleslovas.dapkunas@mif.vu.lt
[2] Institute of Biochemistry, Life Sciences Center, Vilnius University, Sauletekio al. 7, LT-10257 Vilnius, Lithuania; remigijus.simkus@bchi.vu.lt
* Correspondence: romas.baronas@mif.vu.lt

Abstract

This paper analyses the self-organization and spatio-temporal pattern formation in bacterial and human populations using chemotaxis-based mathematical models. The pattern formation in the following three chemotaxis-type systems is investigated: the self-organization of suspensions of luminous *Escherichia coli* bacteria, the capital-induced labor migration in a spatial Solow model, and the movement of urban criminals forming crime hotspots. The three models are selected as representative examples of chemotaxis mechanisms that capture distinct modeling assumptions and applications. Nonlinear two-dimensional as well as one-dimensional-in-space reaction–diffusion–chemotaxis models were used to simulate the pattern formation in all three chemotactic systems within a restricted area—a circle. The models are formulated in dimensionless form, and the corresponding dimensional parameters are estimated through the comparison of simulation results with experimental and statistical data. The numerical simulation under the transient conditions was carried out using the finite difference technique. This study highlights substantial differences between bacterial motility and the geographical movement of humans; however, human populations' movement toward an attractant can be regarded as analogous to the chemotactic behavior of biological cells, differing primarily in scale.

Keywords: chemotaxis; pattern formation; population dynamics; mathematical modeling; bacterial self-organization; capital-induced labor migration; urban crime propagation

MSC: 92-10; 92C17

Academic Editor: Jiashan Zheng

Received: 20 January 2026
Revised: 19 February 2026
Accepted: 21 February 2026
Published: 24 February 2026

1. Introduction

Most living organisms—from bacteria to humans—must migrate in some form to secure favorable conditions [1]. A primary mechanism underlying such directed movement is chemotaxis, the process by which organisms or cells move in response to chemical gradients [2]. In positive chemotaxis, movement occurs toward a chemoattractant, whereas in negative chemotaxis, it is directed away from a chemorepellent. Through this mechanism, cells and organisms sense, respond to, and actively modify the chemical landscape of their environment [2,3]. Chemotaxis is fundamental to a wide range of biological processes essential for health and development, including inflammation, neuronal patterning, wound healing, tumor progression, and embryogenesis [1,3].

In particular, bacterial chemotaxis represents one of the most extensively studied model systems for understanding spatio-temporal pattern formation [2,4,5]. For example, *Escherichia coli* exhibit chemotaxis toward self-excreted attractants, leading to collective behaviors such as swarming and aggregation [4,6]. Bacterial populations often develop in spatially heterogeneous environments, e.g., biofilms, where variations in local density, nutrient availability, and extracellular polymeric substances significantly influence transport processes and collective dynamics [7,8].

Since the work of Keller and Segel [9], mathematical modeling has played a substantial role in the study of chemotaxis [3,5]. Although a number of mathematical models based on partial differential equations have been developed, the system introduced by Keller and Segel remains among the most widely used [3,5,10,11]. Recently, Painter showed [3] an exponential growth in the number of publications and researchers citing the pioneering work of Keller and Segel [9].

In general, models of the Keller–Segel type are appropriate for systems in which motile agents undergo random motion (i.e., diffusion) that is biased by gradients of a self-produced signal, e.g., a chemoattractant [2–4,9].

Using the Keller and Segel approach [9], the dynamics of chemotactic population and the chemoattractant are mathematically modeled by a system of nonlinear equations of the reaction–diffusion–chemotaxis type [4,9]. Although the chemotaxis-type models are still mostly applied in biology, they have also been applied to solve problems in various other fields, including social sciences [3].

Neto and Claeyssen have applied a chemotaxis model to describe economic growth, containing capital-induced labor migration, where greater labor generates more capital and capital attracts labor [3,12,13]. Their model also involves logistic growth for the labor force. The modeling showed how labor and capital together localize and form dominating economies, as well as benefits to the economy due to the formation of economic agglomerations and cycles [12,14].

Since the analysis of residential burglary data showed the formation of high-density clusters, so-called criminal hotspots, over time, Short et al. proposed a chemotaxis-type system to describe the advective movement of criminals toward increasing concentrations of an attractiveness value [15,16]. The study of crime patterns via the use of the chemotaxis-type model has resulted in a lot of convincing research and has shown that the model is adequate to describe the formation of crime hotspots encountered in reality [17–21].

In general, there exist large differences between the diffusion of biological particles and the geographical movement of the human population [22,23]. Recent studies have shown that spatial heterogeneities in corresponding systems may arise from anomalous diffusion [8,24]. A human population migrates over a much larger domain, such as a continent or an intercontinental region, than biological particles, such as a laboratory dish. Nevertheless, Tabata et al. demonstrated that human migration and the diffusion of various biological particles, including cells and bacteria, exhibit close similarities, differing primarily in scale [22]. Tabata et al. used the Fokker–Planck equation in their study [22], which is equivalent to the convection–diffusion equation when applied to particle position distributions. The studies on pattern formation observed in cell populations are applicable also to those on colony formation observed in the migration of the human population [3,22].

The aim of this work was to investigate the chemotaxis-based self-organizing and patterning relationship between bacterial and human populations using chemotaxis-based dimensionless mathematical models and to estimate values of the corresponding dimensional model parameters. As *E. coli* is one of the most studied bacterial examples, the bioluminescence pattern formation in suspensions of lux-gene-engineered *E. coli* near the top surface and near

the three-phase contact line of a right circular container was studied [25–27]. Two aspects of human social behavior were also analyzed: the formation of economic agglomerations, which are regions with higher levels of capital and labor force than their neighbours [12], and the formation of crime hotspots, when criminals move toward a higher concentration of an attractiveness value [15,16].

Nonlinear two-dimensional (2D) as well as one-dimensional-in-space (1D) reaction–diffusion–chemotaxis models were used to simulate the pattern formation in all three chemotactic populations living within a restricted area—a circle [26,27]. Although the overall population behavior in a 1D domain is similar to that in a 2D domain, the 2D simulation provides additional insights to understanding the population behavior [3,7,14,16,28,29], e.g., the spatial agglomerations in 2D can have two different forms, stripes or spots, while in 1D only the spot pattern is possible [14].

By changing the model's parameters, the pattern formation was analyzed with a special emphasis on simulating patterns that were similar across all three chemotactic-like systems of a very different nature. The numerical simulation at the transient conditions was carried out using the finite difference technique [10,27,30].

This paper focuses on a comparative analysis of three representative mathematical frameworks that arise in different biological and social scenarios. Although each model has been studied previously in isolation, a unified analytical and numerical treatment that highlights their similarities, differences, and applicability has been lacking. By examining these models within a single mathematical and computational framework, we clarify how distinct modeling assumptions influence qualitative behaviors such as aggregation, stability, and pattern formation. This perspective is particularly relevant for applications, as it provides guidance on model selection and interpretation in biological contexts. The main contribution of this work is a comparative synthesis of established chemotaxis models, offering new insight into their structure, behavior, and biological relevance.

Although chemotaxis-type models have been extended beyond biology, their systematic application to socio-economic systems remains relatively limited, reflecting the interdisciplinary challenges involved [1,3]. In this work, we deliberately select three representative models to examine how a common chemotaxis-type structure gives rise to aggregation in distinct biological and social contexts. By analyzing these systems within a unified numerical framework, we demonstrate that human mobility can be modeled analogously to bacterial chemotaxis, with movement directed toward socio-economic "attractants" such as higher income, better employment opportunities, or improved social conditions, and away from "repellents" such as high crime rates or poverty. We further identify shared instability mechanisms and essential differences arising from their specific nonlinear interaction terms.

The paper is organised as follows. Section 2 describes the dynamics of the chemotactic population by a generalized Keller–Segel model of chemotaxis as well as by three specific models devoted to bacterial self-organization, capital-induced labor migration, and urban crime propagation. Numerical solution and computer simulation issues are discussed in Section 3. The results of the computational experiments are presented and discussed in Section 4. Finally, the conclusions of the investigation are formulated.

2. Mathematical Models

Real-world statistical processes in human societies are inherently complex and influenced by numerous interacting factors [15,22,23]. To capture this complexity in a tractable way, these processes are often modeled using mean field approaches, typically represented mathematically by systems of partial differential equations [3,12,15,22]. The Keller–Segel model is a widely used mean field model, originally developed to describe

chemotactic aggregation in biological systems [9]. Like other mean field models, the Keller–Segel framework is most appropriate for systems with a very large number of interacting agents, such as bacterial colonies [4,22].

The three models considered in this work were selected as representative examples of chemotaxis mechanisms arising in different biological and social settings. Studying them together allows us to identify common mathematical structures as well as fundamental differences that are often obscured when models are analyzed separately.

2.1. Keller–Segel Model of Chemotaxis

According to the Keller and Segel approach, the chemotaxis model describes the dynamics of a chemotactic population and its attractant or repellent [9,11]. Translating the main biological processes into a mathematical model leads to a system of two coupled reaction–diffusion–advection equations. Rescaling the model's variables and introducing appropriate dimensionless parameters lead to the following system of nonlinear equations in the dimensionless form:

$$\frac{\partial u}{\partial t} = D\Delta u - \nabla \cdot (h(u,v)u\nabla v) + \gamma f(u,v), \tag{1a}$$

$$\frac{\partial v}{\partial t} = \Delta v + \gamma(g_p(u,v) - g_d(u,v)v), \quad \mathrm{x} \in \Omega \subset \mathbb{R}^n, \quad t > 0, \tag{1b}$$

where x and t stand for dimensionless space and time, respectively, $u(\mathrm{x},t)$ denotes the population (cell or organism) density, $v(\mathrm{x},t)$ denotes the attractant (chemical signal) concentration, D is the diffusion coefficient, $f(u,v)$ stands for population growth and death, $h(u,v)$ is the chemotactic sensitivity coefficient, g_p and g_d describe the production and degradation of the attractant, and γ stands for the spatial and temporal scale [4,6,9,28,31]. Instantiating f, g_p, g_d and h with specific expressions leads to a particular models of chemotaxis [3,5,32].

In system (1), the cell density u evolves through the combined effects of random motility, chemotactically directed movement, and local population kinetics. The term $D\Delta u$ represents undirected diffusion, while the flux—$\nabla \cdot (h(u,v)u\nabla v)$ models chemotaxis driven by gradients of the signal v. The reaction term $\gamma f(u,v)$ accounts for local population dynamics. The signal v evolves through diffusion, production, and degradation, as described in (1b).

The complexity of chemotaxis models is often expressed by a signal-dependent chemotactic sensitivity function $h(u,v)$, which controls the chemotactic response of organisms to the attractant [5]. Particularly, logarithmic chemotactic sensitivity assumes that the sensitivity of organisms to an attractant gradient is inversely proportional to the concentration of the chemical [5,17,33]. In the simplest form, the sensitivity of organisms to an attractant is assumed to be independent of the attractant concentration, assuming constant $h(u,v)$ [31].

In the present study, we assume a constant diffusion coefficient D, as is common in many applications [3,5,11], in order to focus on the fundamental interplay between the reaction, diffusion, and advection mechanisms underlying chemotactic aggregation. Nevertheless, spatial heterogeneities may arise from anomalous or non-uniform diffusion in these dynamic systems. Computational models can provide complementary insight into diffusion processes in such complex environments [8,24,34]. From a modeling perspective, environmental heterogeneity can be incorporated by allowing transport coefficients, most notably the diffusion coefficient, to depend explicitly on space and, potentially, on time [8,11,24,34–36]. In some applications of chemotaxis-type models, including bacterial

pattern formation and human population migration, the diffusion term is assumed to depend nonlinearly on the attractant concentration and/or the population density [5,11,29].

Non-dimensionalizing mathematical models is useful for the qualitative analysis of their physical properties, as it expresses both dependent and independent variables in terms of the characteristic limit quantities specific to each system under consideration [11]. Therefore, the formulation of the model in the dimensionless form must be adapted to each case study [11].

The dimensionless form of a model contributes to a deeper understanding of the population's nonlinear dynamics that depend on the specific physical features of the system to be investigated [11]. The main property of the governing Equation (1) is to form spatial patterns of population distribution u when the chemical signal v acts as an attractant, i.e., when population individuals migrate up to gradients of the chemical signal [5].

The chemotaxis model has been applied to investigate the bacterial self-organization in small rounded containers as detected by bioluminescence imaging [25,27,28]. The pattern formation in a colony of luminous *E. coli* was numerically studied in a three-dimensional (3D) domain [27]. It was determined that, due to the accumulation of luminous cells near the top three-phase contact line, the experimental patterns can be simulated with sufficient quality by using one (1D)- and two (2D)-dimensional models [27]. The chemotactic-like social behaviors of human populations are usually computationally modeled in 1D [12,16,37] or 2D [13,14,16,29,35].

To compare the dynamics of bacterial and human populations, the chemotaxis model (1) was applied to 2D (a unit disk Ω_2) and 1D (an interval Ω_1) domains:

$$\Omega_1 = \{x \mid 0 < x < 2\pi\}, \tag{2a}$$

$$\Omega_2 = \{(r,\theta) \mid 0 < r < 1,\ 0 \le \theta < 2\pi\}, \tag{2b}$$

where Ω_1 is the interval corresponding to the circumference of the unit disk Ω_2.

The governing Equation (1) is considered subject to initial and boundary conditions. The following equations provide the initial distributions of the organisms and attractant:

$$u(\mathrm{x},0) = u_0(\mathrm{x}), \quad v(\mathrm{x},0) = v_0(\mathrm{x}), \quad \mathrm{x} \in \Omega. \tag{3}$$

Both functions $u_0(\mathrm{x})$ and $v_0(\mathrm{x})$ are usually assumed to be non-negative. Spatial patterns arise if at least one of the functions $u_0(\mathrm{x})$ or $v_0(\mathrm{x})$ is not constant [5,32,38]. However, most chemotaxis systems exhibit sensitive dependence on the initial conditions. Each initial perturbation can be drastically different from the others, resulting in many distinct spatial patterns [5,32,38].

In the case of the 1D model, the periodic boundary conditions are used because of the continuity of the circle ($t > 0$),

$$u(0,t) = u(2\pi,t), \quad v(0,t) = v(2\pi,t), \tag{4a}$$

$$\left.\frac{\partial u}{\partial x}\right|_{x=0} = \left.\frac{\partial u}{\partial x}\right|_{x=2\pi}, \quad \left.\frac{\partial v}{\partial x}\right|_{x=0} = \left.\frac{\partial v}{\partial x}\right|_{x=2\pi}. \tag{4b}$$

The periodic boundary conditions (4) on the circumference of the disk mean that the boundary is treated as a continuous loop. An organism moving around the circumference will smoothly re-enter from the opposite side, creating a continuous circular path.

In the case of the 2D model, the zero flux boundary conditions are used on the disk edge, while the periodic boundary conditions are imposed on other boundaries ($t > 0$) [26,27]:

$$u(r,0,t) = u(r,2\pi,t), \quad v(r,0,t) = v(r,2\pi,t), \quad r \in [0,1], \tag{5a}$$

$$\frac{\partial u(r,0,t)}{\partial \theta} = \frac{\partial u(r,2\pi,t)}{\partial \theta}, \quad \frac{\partial v(r,0,t)}{\partial \theta} = \frac{\partial v(r,2\pi,t)}{\partial \theta}, \quad r \in [0,1], \tag{5b}$$

$$u(0,\theta,t) = u(0,\theta+\pi,t), \quad v(0,\theta,t) = v(0,\theta+\pi,t), \quad \theta \in [0,\pi], \tag{5c}$$

$$\frac{\partial u(0,\theta,t)}{\partial r} = -\frac{\partial u(0,\theta+\pi,t)}{\partial r}, \quad \frac{\partial v(0,\theta,t)}{\partial r} = -\frac{\partial v(0,\theta+\pi,t)}{\partial r}, \quad \theta \in [0,\pi], \tag{5d}$$

$$\frac{\partial u(1,\theta,t)}{\partial r} = 0, \quad \frac{\partial v(1,\theta,t)}{\partial r} = 0, \quad \theta \in [0,\pi]. \tag{5e}$$

Applying the periodic boundary conditions (5c,d) at the center ($r = 0$) of the disk ensures that the local environment around the center remains continuous, and the population dynamics in the center are modeled as if they were slightly farther away. Similarly, the periodic boundary conditions (5a,b) on the angular coordinate θ implies that organisms moving in the angular direction experience a seamless transition at the boundary where $\theta = 0$ and $\theta = 2\pi$.

Boundary conditions may vary depending on the nature of the population and the shape and size of the area in which the population lives [32,39]. However, the zero flux boundary conditions are most commonly used to model the dynamics of different populations [23,40]. Short et al. imposed a periodic boundary condition in the 1D case and two types of boundary conditions, periodic and zero flux, in the 2D case while analyzing the formation of crime patterns [15,16]. The zero-flux conditions correspond to placing a wall at the border of the domain, preventing the diffusion of both burglars and attractiveness, while periodic conditions are particularly applicable to large spatial domains [40].

Periodic boundary conditions are also often employed in the theory of geographical migration when a population relocates within a bounded domain [23]. Tabata et al. applied periodic boundary conditions to model human migration from sparsely populated areas to densely populated areas [23]. Ispolatov et al. applied these conditions to model the spatially localized competition in geographically structured populations and demonstrated that the formation of multimodal clusters is not an artifact of boundary conditions [41].

2.2. Bacterial Self-Organization

The bacterial growth rate f is mostly modeled by the logistic form [4,5,11,31]. This is also called Keller–Segel system with a Fisher–KPP birth term or Keller–Segel–Fisher system [42]. A population grows logistically when resources are limited. During logistic growth, the population growth decreases due to a lack of resources and levels off when the environmental carrying capacity is reached, resulting in an S-shaped curve [39].

The form of the function $h(u,v)$ ultimately depends on the sensitivity of cells at different concentrations of the attractant [43]. In the modeling of bacterial self-organization, the sensitivity of cells to an attractant is often assumed to be independent of the chemoattractant concentration, i.e., $h(u,v)$ is constant [31].

A number of chemoattractant production functions have been used in chemotactic models [3,5]. Usually, a saturating function of the cell density is used, indicating that, as the cell density increases, the chemoattractant production decreases [9,31,43]. The rate of the attractant's degradation or consumption is typically constant [5,6].

The mathematical model of the bacterial self-organization in a luminous *E. coli* colony was expressed by substituting the following functions into the general form of the model (1):

$$h(u,v) = \chi, \quad f(u,v) = \alpha u(1-u), \quad g_p(u,v) = \frac{u}{1+\beta u}, \quad g_d(u,v) = 1, \tag{6}$$

where u and v denote the dimensionless bacterial density and chemoattractant concentration, respectively, χ is the bacterial chemotactic sensitivity, the function f represents logistic growth for the cell population, α is the dimensionless growth rate constant, and β stands for the saturating signal production. All of the coefficients were assumed to be constant and positive [27,28].

According to the classification of chemotaxis models introduced by Hillen and Painter [5], the model of bacterial pattern formation expressed by (1) and (6) combines two models: the nonlinear signal kinetics model and the cell kinetics model. This model has been analyzed by Maini and others [31,39,43].

A necessary condition for the emergence of spatial patterns is obtained through a standard linear stability analysis of the homogeneous steady state of the 1D model defined by (1) and (6) [5,32,44]:

$$\chi > \left(\sqrt{D} + \sqrt{\alpha}\right)^2 (1+\beta)^2. \tag{7}$$

Notably, this instability criterion is independent of the spatial and temporal scaling parameter γ. Physically, this relationship reflects the mechanism driving bacterial self-organization: a positive feedback between chemoattractant secretion and chemotactic migration can dominate diffusive spreading and density-regulating growth, leading to the amplification of small spatial perturbations and the emergence of stable bacterial aggregations from an initially homogeneous population [32]. When the above inequality is satisfied, chemotactic attraction to the self-produced chemoattractant along the contact line is strong enough to amplify small density fluctuations, destabilizing the homogeneous state and leading to spontaneous bacterial self-organization and the emergence of non-uniform spatio-temporal patterns.

2.3. Capital-Induced Labor Migration

The chemotaxis models have also been applied in the social sciences to describe macroscopic socio-economic phenomena [13,35]. Neto et al. have proposed a model of economic growth that takes into account the migration of both labor and capital, which is assumed to follow a Fourier-type diffusion across space [12,14]. Their model in the dimensionless form reads as (1) with the following specific functional choices:

$$h(u,v) = \chi, \quad f(u,v) = \alpha u(1-u), \quad g_p(u,v) = v^{\phi} u^{1-\phi}, \quad g_d(u,v) = 1, \tag{8}$$

where u and v are the dimensionless densities of labor and capital, respectively, χ is the capital-induced labor migration coefficient, the function f represents the natural growth rate of the labor force assumed to be logistic, involving a dimensionless population growth rate constant α, the function g_p is the Cobb–Douglas capital production function with the output elasticity ϕ of capital (and $1-\phi$ is the output elasticity of labor), the function g_d stands for the capital depreciation, $\chi \geq 0$, $\alpha > 0$, $\phi \in (0,1)$ [12,13,37].

The labor force growth rate is modeled by the logistic function f, just as the bacterial growth rate. The capital-induced labor migration rate h is also assumed to be constant, as in the modeling of bacterial self-organization. Only the capital production rate g_p is significantly different from the bacterial self-excreted attractant production rate. The capital production is modeled by the Cobb–Douglas function of two factors, labor and capital [12], while the corresponding chemoattractant production depends only on one factor, bacteria, as the chemoattractant is self-produced by bacteria [4,6].

Accepting definition (8), the governing Equation (1a) describes the spatio-temporal evolution of labor u, while (1b) describes the spatio-temporal dynamics for the density of capital. This is consistent with neoclassical economic growth when workers move from regions with lower capital density to regions with higher capital density [12,13,37].

The advective term $\nabla \cdot (h(u,v)u\nabla v) = \nabla \cdot (\chi u \nabla v)$ in (1a) models the labor force movement to regions with a higher density of capital, assuming the density of this capital-induced labor migration is proportional to the density $u(\mathrm{x},t)$ of workers living in x [12]. If the capital density $v(\mathrm{x},t)$ at location x is greater than in its neighborhood, neighboring workers will be attracted to move to x with an intensity proportional to the workers $u(\mathrm{x},t)$ living in x, since a greater $u(\mathrm{x},t)$ provides easier access to a larger market. Conversely, if the capital density $v(\mathrm{x},t)$ at location x is lower than in its neighborhood, there will be increased competition among workers at x for the limited capital available. A higher $u(\mathrm{x},t)$ in such a case leads to more competition for jobs and capital, intensifying emigration from x to its surroundings [12].

Originally, the functions g_p and g_d involve the constant factor β of total productivity [12,14]. Here, this proportionality factor is incorporated into the scale parameter γ used in the governing Equation (1). The use of the γ-parameter leads to the introduction of the rate constant α, which is equal to unity in the dimensionless model of Neto et al. [12,14], $\alpha = 1/\beta$.

Whenever $\phi \to 0$, the model given by (1) and (8) reduces to the Keller–Segel model with the cell kinetics model [5].

Balcı used the initial functions $u_0(\mathrm{x},t)$ and $v_0(\mathrm{x},t)$ with respect to the binomial logistic regression model adopted for different countries of the world [37]. The initial Gaussian perturbation of the equilibrium as well as a small random perturbation of the labor and the capital were also used [12].

Several improvements of the model have been proposed. Neto et al. introduced a capital transport cost, and decreasing and increasing returns to scale in the production process [12,14]. Very recently, Ballestra introduced the effect of salaries on the spatial distribution of labor [35]. Balcı proposed to use fractional order derivatives for the time variable instead of usual derivatives, assuming that labor migration and capital flow involve self-similarities in long-range time [24,37]. Nevertheless, functions (6) qualitatively express the main properties of the migration of both labor and capital.

Neto et al. derived an instability condition for capital-induced labor migration [12], which, after being adapted to the formulation given in (1) and (8), reads

$$\chi > \left(\sqrt{D(1-\phi)} + \sqrt{\alpha}\right)^2 / (1-\phi). \tag{9}$$

From an economic perspective, this result indicates that the model can generate economic agglomerations or spatio-temporal cycles only when the capital-induced labor migration is sufficiently strong [14].

2.4. Urban Crime Propagation

Short et al. have proposed a chemotaxis-type system for modeling the formation of high-density clusters, so-called criminal hotspots, observed in the time evolution of residential burglary data [15,16]. The system reflects the advective movement of criminals toward the increasing concentration of an attractiveness.

The model proposed by Short et al. has been intensively analyzed and modified, for instance in [17,19,29,33,40,45]. Rodriguez and Bertozzi have introduced linear functions instead of the logarithmic function of the attractiveness sensitivity and the nonlinear function of the attractiveness value increase [18]. Heihoff has incorporated the logistic source function into the equation [45]. Nevertheless, the model proposed by Short et al. describes the main features of criminal qualitative behavior, which is expressed by spatio-temporal collections of criminal activities (hotspots) [3,15,18]. The model for crime

hotspot formation in a dimensionless form can be expressed by (1), together with the following functions [15,16]:

$$\begin{aligned} h(u,v) &= \frac{\chi}{k_2+v}, \quad f(u,v) = k_1 - (k_2+v)u, \\ g_p(u,v) &= (k_2+v)u, \quad g_d(u,v) = 1, \end{aligned} \tag{10}$$

where $u(\mathrm{x},t)$ represents the density of criminal population (criminal agents), $v(\mathrm{x},t)$ denotes the abstract so-called attractiveness value (factor) for criminal activity, χ stands for the velocity of advective movement of criminals toward increasing concentrations of an attractiveness value, and $k_1(\mathrm{x})$ and $k_2(\mathrm{x})$ denote the density of additional criminals and the source of attractiveness, respectively, $\chi > 0$, $k_1 \geq 0$ and $k_2 \geq 0$.

Short et al. demonstrated that the nonlinear system (1) with functions (10) describes the pattern formations that qualitatively capture the features and dynamics of the urban residential burglary aggregates (crime hotspots), which are presented in the form of spiky steady states of urban residential burglaries [15].

The advective term in (1a) describes the movement of the criminal population toward regions with a higher density of house attractiveness. Crime hotspots refer to the clustering of crime data in urban residential burglaries, where some neighborhoods have higher crime rates and are surrounded by neighborhoods with lower crime rates [15,16,19].

The attractivity function $h = \chi/(k_2+v)$ models the sensitivity of criminals to the attractiveness value and represents the response of the criminals to the concentration v of the attractiveness value in the environment. χ determines the scaling factor or the maximum value of the sensitivity to the attractant. k_2 is a threshold value of the attractant concentration. This term helps set the point at which the criminals' sensitivity to the attractiveness value starts to decrease significantly. As the concentration v decreases, the sensitivity increases and approaches a maximum value χ/k_2; the sensitivity is independent of the attractant in the modeling of both bacterial self-organization and capital-induced labor migration.

According to (10) the attractivity h is decomposed into the background level (k_2) and the dynamic component (v), while it was assumed to be constant when modeling bacterial self-organization and capital-induced labor migration. The attractivity h is a monotonically decreasing function of the distance that criminals travel away from their primary residence to engage in crime decreases [15].

The density u of the criminal population decreases at the same rate $(k_2+v)u$ as the attractiveness value increases; in other words, crime in an area increases attractiveness and reduces recidivism [11,45]. The function f includes specific information about criminals' growth, expressed as k_1, independent of the model functions u and v, such as the socio-economic status of certain urban areas at certain points in time that affect criminalization [15].

Originally, Short et al. used a particular value of the sensitivity $\chi = 2$, and the gradient $\nabla(k_2+v)$ was used instead of ∇v [15,16]. However, the functions k_1 and k_2 can be reasonably assumed to be constant and then $\nabla(k_2+v)$ reduces to ∇v [3,29,36].

Both versions of the attractant production function g_p, the Cobb–Douglas function with unitary output elasticity sum used in modeling the capital-induced labor migration, and the logistic-type saturating signal production function used in modeling the bacterial self-organization, describe growth processes that incorporate inherent constraints, albeit in different ways. In bacterial populations, the logistic-type saturation function models growth that is constrained by resource limitations. The system is inherently self-limiting. The Cobb–Douglas function, when the sum of output elasticities equals one, describes a

scale-invariant process, where the output grows proportionally with the inputs, without intrinsic saturation.

Short et al. showed that crime hotspot formation in system (1) with reaction terms (10) may result from a linear instability of the spatially homogeneous steady state [15,16]. In particular, they derived the following instability criterion, which, when adapted to the model formulation (1) and (10), takes the form

$$\chi > \left((k_1 + k_2)^2 + Dk_2 + 2\sqrt{D(k_1 + k_2)^3} \right) / k_1 \,. \tag{11}$$

This condition expresses that hotspots emerge when the aggregation of criminals driven by their response to local crime intensity overwhelms the combined stabilizing effects of random criminal motion, law-enforcement-induced removal, and crime decay over a finite spatial scale [15,16]. Mathematically, it requires that chemotactic drift dominate diffusive spreading and that the local crime–criminal feedback be sufficiently strong to sustain the growth of spatially localized perturbations.

In numerical simulations, the initial data were a small perturbation or a mild concentration of both the criminal population and the attractiveness value [29,36]. However, due to the specific functional choices (10), spatial patterns (hotspots) could emerge even with an initial uniform distribution of attractiveness [3,15].

Numerical analysis by Short et al. showed, in particular, that subcritical crime hotspots may be permanently eradicated with police suppression, whereas supercritical hotspots are displaced following a characteristic spatial pattern [16]. Their findings qualitatively explain failures to observe crime displacement in experimental field tests of hotspot policing [16]. Although the concept of attractiveness is difficult to quantify, model simulations showed that empirical data can lead to the formation of complex hotspots and provide a means for effectively deploying anti-crime measures [3,15].

2.5. Dimensionalizing the Variables

A dimensionless mathematical model aims to define the main governing parameters of the dimensional mathematical model [5,39,43]. The scale parameter γ can be used to simulate domains of different sizes [31].

Values of the dimensionless parameters are often determined experimentally by varying the input parameters, aiming to simulate patterns comparable to the experimentally obtained patterns [3,28]. Nevertheless, the dimensionless parameters should be validated to ensure that the corresponding dimensional parameters have physical meaning.

The Keller–Segel model is usually non-dimensionalized by introducing the dimensionless space and time parameters, assuming the constant dimensional rate $g_d^* = a$ of the attractant degradation, where a is the rate constant, $a > 0$. In such a case, the dimensionless time t, space variables r, θ, x, and the dimensionless diffusion coefficient D are defined as follows:

$$t = \frac{at^*}{\gamma}, \quad r = \sqrt{\frac{a}{D_c\gamma}}r^*, \quad x = \sqrt{\frac{a}{D_c\gamma}}x^*, \quad \theta = \theta^*, \quad D = \frac{D_n}{D_c}, \tag{12}$$

where t^*, r^*, θ^* and x^* are the corresponding time and space dimensional parameters, and D_n and D_c are the dimensional diffusion coefficients of the population and attractant, respectively. According to the parameter transformation (12), the relation between dimensionless time t and space variables r (2D model) and x (1D model) is invariant to the parameters a and γ:

$$t = \left(\frac{r}{r^*}\right)^2 D_c\, t^*, \quad t = \left(\frac{x}{x^*}\right)^2 D_c\, t^*. \tag{13}$$

The dimensional size of the domain, the duration of the process, and the diffusion coefficients are among the most easily determined parameters by physical experiments. The transformation of the other model parameters is more complicated and depends on the form of the functions $f(u, v)$ and $g_p(u, v)$, which vary notably in specific models (6)–(10), and in most cases, their values are not precisely determined [6]. Because of this, the numerical results are analyzed below in terms of dimensional space, time, and diffusion, taking into consideration the transformation (12).

Assuming that R^* is the dimensional radius of the physical disk being modeled, T^* is the duration of the modeled process on the disk, and T is the corresponding dimensionless duration, the diffusion coefficients D_c and D_n can be equally calculated from (12) for both 1D and 2D models and then compared with the corresponding known diffusion coefficients,

$$D_c = \frac{T}{T^*} R^{*2}, \quad D_n = D\, D_c. \tag{14}$$

On the other side, with an estimation of at least one one-dimensional diffusion coefficient D_n or D_c applicable to a chemotaxis-based system, the size (radius R^*) of the physical domain and the simulation time T, formula (14) allows us to calculate the physical process duration T^* required for the modeled population to undergo structural changes similar to the modeled pattern changes over time T.

3. Numerical Simulation

The Keller–Segel model of chemotaxis admits analytical solutions only in a few special or simplified cases, predominantly in one spatial dimension [10,11]. Consequently, chemotaxis-type models are most often studied using numerical methods based on a variety of computational techniques [5,14,24,28,32,35,44,46].

Due to the nonlinearity of the governing Equation (1), the initial boundary value problem (1)–(5) was solved numerically using the finite difference method [30]. An explicit finite difference scheme has been built as a result of the difference approximation [10,30]. Although more complex, robust, and efficient algorithms can be developed by using domain decomposition and splitting in space methods [44], the simpler-to-program explicit method proved to be efficient enough [46].

All the forcing functions h, f, g_p, and g_d were also treated explicitly in time. This explicit treatment was chosen to ensure consistency with the overall time-stepping scheme used in our models and to maintain computational efficiency. The approach yielded stable, accurate results across the parameter and time-step ranges used in our simulations.

To find a numerical solution of the problem, a discrete uniform grid in space and time was used. Since the dimensionless diffusion coefficient D, the chemotactic sensitivity coefficient χ and the scale parameter γ for modeling using (10) were one to two orders of magnitude larger than those used for modeling the other two systems, a significantly denser grid was required to accurately simulate the urban crime propagation. The discrete space grid sizes and time step sizes used in all the simulations are defined in Table 1.

Table 1. Model parameter values, discrete space grid size, time step size τ, and duration T of the simulated bacterial self-organization (Bacteria) [25,27,47], labor migration (Labor) [12,24], and urban crime propagation (Crime) [3].

Parameter	Bacteria		Labor		Crime	
	1D	2D	1D	2D	1D	2D
D	0.1		1		50	
χ	6.0		10		100	
α	1.0		0.4		–	
β	0.7		–		–	
γ	12	36	70	70	600	1500
ϕ	–		0.7		–	
k_1	–		–		10.0	
k_2	–		–		0.5	
$\bar{u}_0$	1.0		1.0		1.0	
$\bar{v}_0$	1.0		1.0		1.0	
N_x, $N_r \times N_\theta$	150	60×70	150	50×150	300	150×250
τ	10^{-5}	5×10^{-8}	10^{-4}	5×10^{-8}	10^{-6}	10^{-10}
T	35.0	12.0	10.0	7.0	0.015	0.01

Another challenge in solving the problem was the singularity at the center of the polar grid for the Laplacian in polar coordinates [48]. In addition, the time step size is affected by the concentration gradient, which can be particularly large in 2D simulations as the 2D spatial agglomerations can have two different shapes, stripes or spots, while in 1D only the spot pattern is possible [14].

The digital simulator was programmed by the authors in Java [49]. The common Keller–Segel model was defined as an abstract class, and two versions, 1D and 2D, of the common model were implemented as subclasses. As commonly used functions, f, g_p, g_d, and h have to be implemented differently, and an interface as a fully abstract class with the corresponding four abstract methods was initially defined and used as a parameter in both versions of the common model. This interface class was then implemented as three different classes implementing those four methods as defined in (6), (8) and (10), respectively. Finally, 1D and 2D models, as two Java classes, were used in conjunction with each of the implementations of three specific models (classes implementing functions f, g_p, g_d and h). The simulation results have been visualized using Origin [50].

Non-uniform distributions of both the chemotactic population and the attractant were used in the initial conditions ($t = 0$):

$$u_0(\mathrm{x}) = \bar{u}_0(1 + \xi_u(\mathrm{x})), \quad v_0(\mathrm{x}) = \bar{v}_0(1 + \xi_v(\mathrm{x})), \quad \mathrm{x} \in \Omega. \tag{15}$$

where $\bar{u}_0$ is the initial average density of cells, $\bar{v}_0$ is the initial average concentration of attractant, and ξ_u and ξ_v are independent random spatial 5% perturbations with a zero average [7,27,28]. The perturbations were applied by sampling values from a Gaussian distribution with a mean of 0.0 and a standard deviation of 0.05 [49]. In all the simulations, a unit mean for both cells and attractant was used, $\bar{u}_0 = \bar{v}_0 = 1$.

To evaluate the coincidence of two versions of the model (1), 1D and 2D, the spatio-temporal patterns near the disk edge were simulated not only using 1D but also using the 2D polar model. To simulate the spatio-temporal patterns of the quasi-one-dimensional population density near the contact line by applying the 2D model, the density u was integrated over a thin ring close to the outer boundary of the thickness δ and then averaged:

$$u_r(\theta, t) = \frac{2}{1 - (1 - \delta)^2} \int_{1-\delta}^{1} u(r, \theta, t) r \mathrm{d}r, \quad \theta \in [0, 2\pi], \ t > 0. \tag{16}$$

The thickness $\delta = 0.02$ (2% of the radius length) was used in all the numerical simulations.

The mathematical model and the corresponding numerical model were mainly validated by computational simulation of bioluminescence patterns observed in small circular containers made of clear glass [25,28,47,51]. Figure 1 shows a typical top view of the experimental culture together with a spatio-temporal plot of the bioluminescence near the three-phase contact line. Published spatio-temporal patterns of capital-induced labor migration were also used for the model's validation [12].

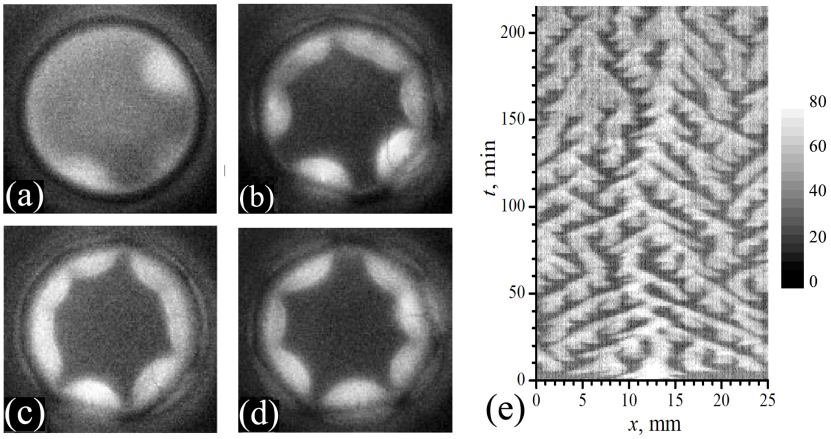

Figure 1. Top view bioluminescence images of the bacterial cultures in the cylindrical container taken at four time moments, 10 (**a**), 30 (**b**), 50 (**c**), and 70 (**d**) minutes, and the space–time plot measured along the contact line (**e**). Adapted from [25,51], with permission from the respective publishers.

Physical experiments with luminous *E. coli* in the rounded containers showed an accumulation of cells near the edge of the top surface, and, because of this, the formation of experimental spatio-temporal patterns was qualitatively simulated by using 1D model [47]. Neto et al. have simulated similar spatio-temporal patterns by using 1D capital-induced labor migration [12]. To evaluate the level of cell accumulation near the edge of the disk, the distribution of the population concentration along the radius of the disk was calculated from the results of the 2D simulation. The density u was integrated over a circle at each radius point and then averaged. Since the population density near the center of the disk varies drastically with time, this density was again integrated over time and then averaged. The average concentration $u_{\theta t}(r)$ as a function of radius is expressed as follows:

$$u_{\theta t}(r) = \frac{1}{2\pi T} \int_0^T \int_0^{2\pi} u(r,\theta,t)\, \mathrm{d}\theta \mathrm{d}t, \quad r \in [0,1], \tag{17}$$

where T is the duration of the simulated process.

In the case of the 1D modeling, the corresponding average concentration $u_t(x)$ on a circle is expressed as follows:

$$u_t(x) = \frac{1}{T} \int_0^T u(x,t)\, \mathrm{d}t, \quad x \in [0,2\pi]. \tag{18}$$

4. Results and Discussion

The nonlinear mathematical model (1)–(5) was used to simulate the pattern formation applying different forms of the functions f, g_p, g_d, and h as defined in (6), (8) and (10).

The simulation was performed using both 1D and 2D versions of the model at the same values of the model parameters, except for the scale parameter γ. Since the first polar coordinate r in the 2D model is scaled the same way as the coordinate in 1D model, and the second polar coordinate θ is not scaled in the 2D model, the scale parameter γ was different in the 1D and 2D simulations, while the values of the other parameters were

unchanged. The simulation results are depicted in Figures 2–4. The numerical experiments were performed using the parameter values listed in Table 1.

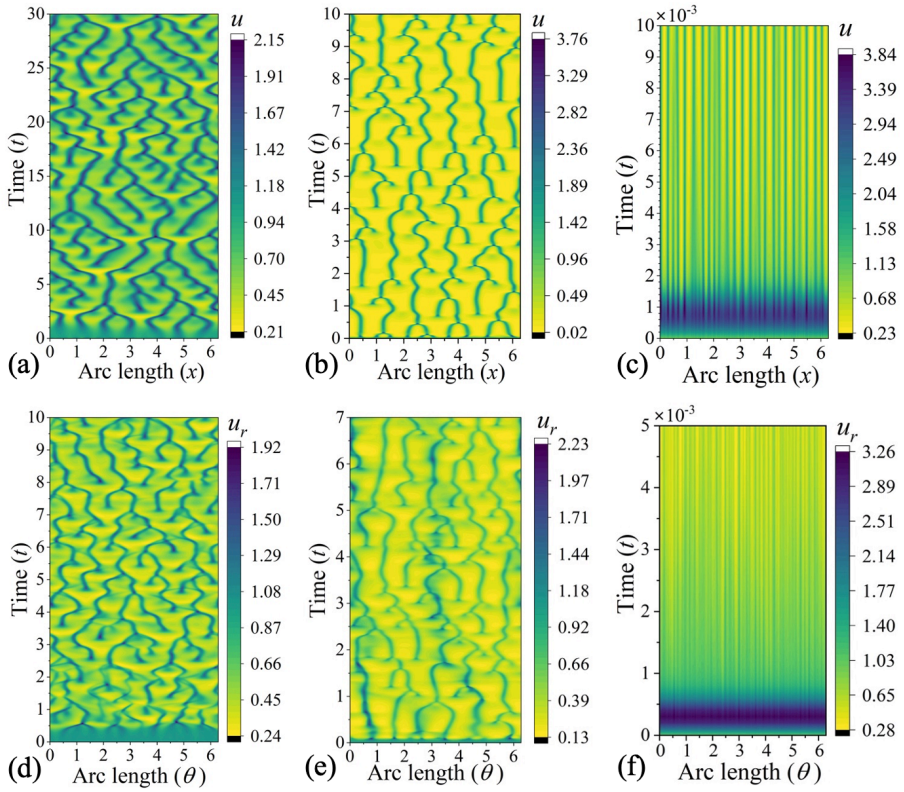

Figure 2. Space–time plots along the contact line simulated by 1D (**a**–**c**) and 2D (**d**–**f**) models of bacterial self-organization (**a**,**d**), capital-induced labor migration (**b**,**e**), and urban crime propagation (**c**,**f**). The dimensional length is obtained by multiplying the dimensionless length by 4 mm (**a**,**d**), 9000 km (**b**,**e**), and 6.15 km (**c**,**f**). The dimensional time is calculated by multiplying the dimensionless time by 7.23 min (**a**), 5 years (**b**), 3.79×10^5 days (**c**), 21.7 min (**d**), 7.14 years (**e**), and 7.57×10^5 days (**f**). Values of u_r from the 2D model were computed using (16).

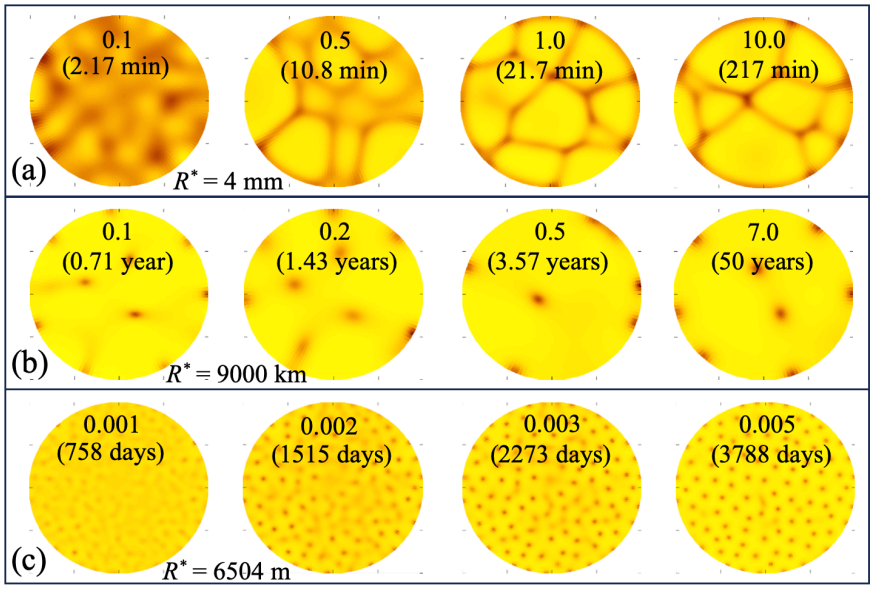

Figure 3. Top views of population densities simulated by 2D models of bacterial self-organization (**a**), capital-induced labor migration (**b**), and urban crime propagation (**c**). Dimensionless and dimensional time moments, as well as the dimensional radius R^*, are indicated within the images.

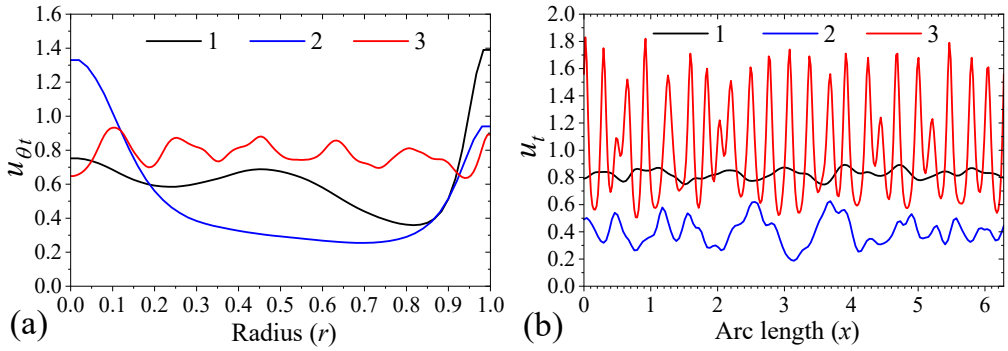

Figure 4. Average population densities $u_{\theta t}$ as a function of radius r (**a**), obtained from 2D models and integrated over time and along the circle of radius r, and u_t on the circle (**b**), obtained from 1D models and integrated over time. The results are shown for bacterial self-organization (1), capital-induced labor migration (2), and urban crime propagation (3).

4.1. Results of Numerical Experiments

The specific functions (6) were used to study the bacterial self-organization in a colony of luminous *E. coli* [25,26]. By varying the model's parameters, the simulation results were analyzed to achieve irregular-wave spatio-temporal patterns comparable to those shown in Figure 1, assuming approximately 13–16 temporal and 6–7 spatial periodical cell accumulations.

The bacterial patterns have been simulated at different values of the model parameters. Particularly, the dimensionless diffusion coefficient D varied from 0.04 [28] to 0.31 [26]. Figures 2a,d, 3a and 4 (curves 1) show typical simulation results at an intermediate value of the dimensionless diffusion coefficient $D = 0.1$ [5,25]. Assuming $D = 0.1$ and the remaining parameter values listed in Table 1, the instability condition (7) for the emergence of spatial patterns reduces to $\chi > 5.0$.

The specific functions (8) were used to simulate the capital-induced labor mobility in the spatial Solow model for economic growth [12,14]. The mathematical model defined in a 2D domain (unit disk Ω_2) describes the migration of labor and capital in a circular closed area, while the model defined in the 1D domain (interval Ω_1) expresses the migration on the boundary of the 2D area (the circumference of the circle).

The simulation of the labor mobility was performed at the model parameter values used by Neto and Claeyssen in [12], where the corresponding model was defined in the 1D domain, a closed interval, applying no-leak boundary conditions defined on both sides of the interval. Zero-flux boundary conditions restrict any migration outside the interval, which economically means that the spatial economy is considered to be an autarchy [14]. The domains Ω_1 and Ω_2 defined in (2) can also be economically considered an autarchy. However, migration in the 1D domain Ω_1 is protected from specific locations such as borders, where accumulations of migrators can be predicted, as Ω_1 is a continuous circle due to periodic boundary conditions (4).

For the application of the capital-induced labor migration model to real data, the scale parameter γ was chosen to generate approximately six spatial accumulations, corresponding to migration from Türkiye to six Western economies over the period 1966–2014 [24,37].

Neto et al. showed that, by varying the model's parameters, the chemotaxis-based spatial Solow model can generate a wide range of spatio-temporal dynamics [12,14]. In particular, they found that moderate capital-induced labor migration ($\chi = 5$) leads to the formation of economic agglomerations, whereas higher migration intensity ($\chi = 10$) can produce periodic or non-periodic spatio-temporal cycles, with peaks of capital and labor propagating through space over time. To capture the spatio-temporal cycles associated with

the large-scale migration from Türkiye to Western economies during the first and second oil crisis periods [24], we therefore set $\chi = 10$. Notably, the instability condition (9) for the capital-induced labor migration is satified when $\chi > 4.64$, given the parameter values in Table 1.

The dimensionless mathematical model defined by (1)–(5) and (10) was used to simulate emerging criminal hotspots within a spatial region roughly outlining Edinburgh [3]. The simulation was performed with the model parameter values defined in [3], transformed into dimensionless form.

When modeling criminal activities in a city, for simplicity, it is reasonable to consider a unit circle (Ω_2) whose area is equal to the city area. An application of no-flux boundary conditions (5e) assumes that the criminals entering the city and the criminal leaving are approximately the same [18]. The value of the scale parameter γ was chosen so that the unit circle corresponds to a dimensional circle whose area is approximately equal to that of Edinburgh.

Relatively high values of the diffusion coefficient $D = 50$ and of the advective velocity $\chi = 100$ for criminal movement were chosen to generate approximately 100 hotspots in Edinburgh within a 2D domain, including about 20 hotspots located along the city boundary, which is represented as a 1D domain, as reported by Painter [3]. In addition, the parameter values used in the simulations (Table 1) correspond to a stationary, non-homogeneous solution, which is typical for the chemotactic-type system developed by Short et al. [15,18,29] and employed in [3]. At these parameter values, the instability condition (11) governing crime hotspot formation reduces to $\chi > 61.6$.

4.2. Estimation of Dimensional Parameters

Using a known inner radius $R^* = 4$ mm of the vessel used in the physical experiment with luminous *E. coli* and the duration $T^* = 1.3 \times 10^4$ s of the experiment [51], the dimensional diffusion coefficients D_c and D_n can be calculated using (14). Taking into account the dimensionless process duration T depicted in Figure 2a,d ($T = 30$ in 1D and $T = 10$ in 2D), $D_c = 3.69 \times 10^{-4}$ cm^2/s and $D_n = 3.69 \times 10^{-5}$ cm^2/s for the 1D simulation, and $D_c = 1.23 \times 10^{-4}$ cm^2/s and $D_n = 1.23 \times 10^{-5}$ cm^2/s for the 2D simulation.

Similar bacterial patterns were also simulated at other values of the model parameters, e.g., at $D = 0.31$, $\chi = 10.5$, $\beta = 0.95$, $\alpha = 1$ and $\gamma = 20$ in 1D, $\gamma = 60$ in the 2D simulation [26]. As the dimensionless duration of the simulated experiment at $D = 0.31$ was the same as that at $D = 0.1$, the calculated dimensional diffusion coefficient D_c is also the same as at $D = 0.1$. However, the dimensional bacterial diffusion coefficient is then 3.1 times larger, $D_n = 1.14 \times 10^{-4}$ cm^2/s for 1D simulation and $D_n = 3.82 \times 10^{-5}$ cm^2/s for 2D simulation.

The estimations of the diffusion coefficients of the chemoattractant and cells can be found in the literature, typically, $D_c = 10^{-5}$ cm^2/s and $D_n = 6.6 \times 10^{-6}$ cm^2/s [52], though several times lower as well as higher values of these coefficients were also published [53,54]. These values of the diffusion coefficients differ from those calculated using (14), but the value of $D_n = 1.23 \times 10^{-5}$ cm^2/s, calculated for the dimensionless coefficient $D = 0.1$, is closer to the typical values found in the literature than those calculated for $D = 0.31$. The fact that the values of both dimensional diffusion coefficients, D_c and D_n, calculated using the 2D model are closer to typical values than those obtained using the 1D model confirms that the 2D model describes the physical process more precisely than the corresponding 1D model.

The simulation results presented in Figure 2b,d for the capital-induced labor migration cover a relatively long period, during which labor accumulations return to the same space position. Published experimental data on labor migration from Türkiye to six Western

economic countries show a gap of about 5–10 years between two peaks of migration numbers [24]. Figure 2b,e show approximately six spatial accumulations similarly to six target countries of the migration from Türkiye. As one can see in Figure 2b, the dimensionless time period between two peaks is about 1–2 dimensionless time units. The radius of a hypothetical circle covering six countries (Australia, Austria, the Netherlands, France, Belgium, and Germany) equals about 9000 km.

Using the radius $R^* = 9000$ km of the geographical area covering those six countries and the statistical duration T^* of 5–10 years that corresponds to the dimensionless duration T of 1–2 units, the dimensional diffusion coefficients D_c and D_n of capital and labor can be calculated using (14): $D_c = D_n \approx 1/5 \times R^{*2} = 16.2 \times 10^6$ km^2/year for the 1D simulation. This diffusion coefficient value corresponds to an annual labor force migration distance of approximately 5700 km ($\sqrt{2D_n t^*}$, assuming $t^* = 1$ year). Since that labor migration velocity was calculated for a few distant countries, it can be considered rather similar to the average global migration distance of 2992–3657 km in 1960–2000 [55].

Although the global labor migration is very different at scale from the bacterial movement in a vessel, the patterns depicted in Figure 2b,e can also be applied for the analysis of the bacterial self-organization, as the patterns were simulated using the dimensionless model. Particularly, the distribution of labor accumulations near the disk edge in 2D simulated patterns (Figure 3b) are especially similar to the experimental patterns (Figure 1b–d) observed in an *E. coli* population.

Using the dimensionless duration T of the capital-induced labor migration depicted in Figure 2b,e ($T = 10$ in 1D and $T = 7$ in 2D) and combining them with the parameters of the physical experiment with an *E. coli* colony ($R^* = 4$ mm and $T^* = 1.3 \times 10^4$ s) shown in Figure 1, the dimensional diffusion coefficient D_n of bacteria can be evaluated using (14), which is invariant to the spatial and temporal scale, $D_n = D_c = 1.23 \times 10^{-4}$ cm^2/s for the 1D simulation and $D_n = D_c = 8.62 \times 10^{-5}$ cm^2/s for the 2D simulation. These values of the diffusion coefficients are comparable to those obtained in the previous section when analyzing the bacterial pattern formation (Figure 2a,d).

In spite of the similarity between bacterial self-organization and the capital-induced geographical movement of the labor force, there are significant differences. Nevertheless, methods and ideas developed in studies on the pattern formation observed in colonies of biological particles are also applicable to colony formation observed in the migration of a human population [22].

Painter used a dimensional chemotaxis-type model for simulating the dynamics of criminal density in Edinburgh, but the parameter values were given without units [3]. Assuming that S is the known area of the city, a circle whose area coincides with the city area has a radius $R^* = \sqrt{S/\pi}$, and the dimensional time T^* required for crime hotspots to develop equals $(S/\pi)T/D_c$, as defined in (14), where T is the dimensionless time of the hotspots' formation.

Figure 2c,f show that crime hotspots are completely formed in about $T = 0.01$ dimensionless time units. According to Wikipedia, the area S of the city of Edinburgh is 119 km^2. Assuming $D_c = 100$ m^2/day is the dimensional diffusion coefficient of the crime attractant [3], the calculated dimensional formation time T^* of crime hotspots in Edinburgh is approximately 3788 days. This time matches with the time 4000 given by Painter with no dimension [3]. The number of hotspots in Figure 3c is also approximately the same (about 100) as in [3], including nearly 20 hotspots on the border of the city.

Neto et al. applied a chemotaxis-based model to qualitatively study the formation of aggregations of gross domestic product (GDP) and population in Brazil [12]. The results of the 1D simulation of the spatio-temporal evolution of capital and workers densities were compared with sliced latitudinal and longitudinal distributions of aggregated per

capita GDP and population in Brazil. Although the spatio-temporal evolution of these two variables was simulated, only the final number of the aggregations was compared with data from the 2010 census.

The simulation by Neto et al. [12] was performed at a constant capital-induced labor migration coefficient $\chi = 10$ and a dimensionless diffusion coefficient $D = 1$ as in our numerical experiments depicted in Figure 2b. The simulated solution contained approximately the same number of peaks as in Figure 2b.

Using an effective radius $R^* \approx 2700$ km, obtained by approximating the geographical area of Brazil as an area-equivalent circular domain, and adopting the capital depreciation (chemoattractant degradation) rate $a = 0.05$/year used in [12], the dimensional diffusion coefficients D_c and D_n can be calculated using the parameter transformation (12) as $D_n = D_c = aR^{*2}/(R^2\gamma) = 5200$ km^2/year. The corresponding annual population migration distance is approximately 102 km. These values are considerably less than those obtained for labor migration from Türkiye to six Western countries, as domestic migration distances are shorter than international migration distances. The calculated velocity of 102 km/year for population migration in Brazil is comparable with the median migration distance of 120 km in Brazil during 2011–2015 [56].

The results of numerical simulation helped Neto et al. demonstrate, in particular, that increasing returns to scale play a crucial role in the formation of economic agglomerations and that higher returns to scale can contribute to a higher aggregate per capita output for the economy as a whole [12]. They also derived a critical value for the capital transport cost, below which the economy develops stably and converges to a spatially homogeneous steady state, otherwise [12] modeling a real urban area with a circle is a fairly rough approximation.

However, the circle can be used to investigate the dynamics of the crime hotspot formation and to estimate values of the dimensional parameters. Moreover, the simulation of a dynamic process in a regular domain, such as a circle, is much simpler than in a domain close to a real city area.

4.3. Inhomogeneities in Population Densities

One can see in Figures 2a,d and 3a the simulated bacterial spatio-temporal patterns near the disk edge, as well as inside the disk similar to the corresponding patterns observed in the physical experiment with luminous *E. coli* (Figure 1). A valuable accumulation of cells near the disk edge (at $r = 1$) is particularly prominent in Figure 4a (curve 1). Although the largest concentration of cells appears on the outskirts of the disk, smaller accumulations are observed approximately halfway ($r \approx 0.45$) between the center and the edge of the disk as well as at the disk center ($r = 0$). Similar peaks have also been observed in snapshots of bacterial density on the inner lateral surface of the vessel [28].

Labor force also accumulates near the edge ($r = 1$) of the area and in the disk center ($r = 0$) similarly to the bacteria population (Figure 4a (curves 1 and 2)). However, the labor force concentration predominates in the center while the bacterial concentration predominates on the edge of the disk. The accumulation of labor at the disk center can also be easily observed in Figure 3b.

Figures 2c,f and 3c show an approximately uniform distribution of crime hotspots in the disk area, including its edge. However, according to Figure 4a (curve 3), the disk edge ($r = 1$) and the area near the disk center ($r \approx 0.1$) are slightly more attractive to criminals than other areas, as those two areas have the highest peaks. The average distribution of criminals $u_{\theta t}$ across the disk radius shows six peaks (Figure 4a) (curve 3). That number can be used to estimate the total number of peaks (hotspots) in the disk, which is approximately equal to $6^2\pi \approx 113$. The number of hotspots is only slightly higher than the number of hotspots shown in Figure 3c.

Figure 4b (curve 1) shows seven main concentration peaks as in the initial phase of the 1D simulation (Figure 2a, $t = 2$). Although the cell accumulations constantly change, the profile u_t of the cell concentrations, averaged over time, still shows peaks approximately at the same positions where those spots originally formed. A similar behavior of clusters also appears for labor force migration (Figures 2b and 4b (curve 2)). This means that population clusters mainly fluctuate around their position rather than traveling freely around the boundary of a closed area. This phenomenon can also be noticed in the experimental spatio-temporal pattern depicted in Figure 1e and in other published patterns [28,47].

The amplitude of the fluctuations depends on the model's parameters. Fluctuations in the calculated average labor density u_t are of noticeably higher amplitude (Figure 4b, curve 2) than in the corresponding bacterial density (Figure 4b, curve 1). The average labor density u_t varies between 0.19 and 0.63 (Figure 4b, curve 2), while the corresponding bacterial density only varies from 0.75 to 0.89, but at higher values of the bacterial density (Figure 4b, curve 1). Figures 4b (curve 3) and 2c show that in a specific case, such as the formation of crime hotspots, the fluctuations vanish, and the system approaches a steady state.

A stationary and spatially non-homogeneous solution is typical for the chemotaxis-type system developed by Short et al. [15,16,18,29], while the spatio-temporal patterns shown in Figure 2a,b,d,e can be characterised by irregular azimuthal waves and the relative stability of the corresponding wave number (number of waves along the contact line). Later modifications of the model of Short et al. were based on different assumptions of criminal behavior, e.g., criminals might have a tendency to avoid regions with a high density of other criminals due to policing, which leads to a non-stationary problem solution [19–21,40].

The non-stationary solution of the chemotaxis-type model corresponds to a nomadic population (Figures 2a,b,d,e and 3a,b) while the stationary solution represents a sedentary population (Figures 2c,f and 3c) [57]. Both types of population behavior are common for both bacterial and human populations. Understanding the social behavior of bacterial populations is of crucial importance for solving different problems, including ecology [57].

Figure 4 shows that population accumulations tend to be evenly distributed in both coordinates, radial and azimuthal. This means that populations tend to maintain approximately equal distances between clusters. The significant difference in the profiles of $u_{\theta t}$ and u_t (Figure 4) can mainly be explained by the difference in the boundary conditions (4a) and (5e), the first being periodic while the other zero flux. The no-leak condition on the boundary results in the accumulation of cells on that boundary due to the chemotaxis, while the periodic boundary condition implies that organisms move freely at that boundary.

The simulation results qualitatively show that the bacterial concentration is highest at the boundary of the domain (Figure 4a, curve 1), although the aggregations of the bacterial population appear to be evenly distributed within the domain (Figure 3a). The labor force is concentrated in the central area (e.g., the capital) and in peripheral regions (e.g., ports) (Figure 4a, curve 2). Crime hotspots emerge even with an initially small perturbation in both the criminal population and the attractiveness value and tend to distribute evenly across the region (Figure 4a, curve 3). Hotspots can occur in cities even in the absence of historically established crime neighborhoods (Figure 3c).

4.4. Validation of Chemotaxis-Type Models

Most organisms on Earth—from bacteria to humans—need to migrate in some form to seek favorable conditions [1]. As shown above, many achieve this through chemotaxis, whereby movement is directed by gradients in environmental factors. Chemotaxis-type models span mathematical, chemical, and physical formulations, providing alternative

abstractions of movement-driven processes across scales, from molecular regulation to the collective dynamics of large populations [1]. The Keller–Segel model and its extensions have been widely applied, often alongside physical experiments, to phenomena ranging from bacterial motion to social behavior [3]. However, model validation remains challenging due to substantial variability in experimental designs, system scales, and underlying signaling and search strategies [1].

A limitation of this study is the lack of detailed external validation using independent empirical datasets for the human migration and crime models, which restricts the generalizability of the findings.

Future quantitative validation could involve comparing the spatial and temporal patterns produced by the reaction-diffusion-chemotaxis models with those derived from independent empirical datasets. For the labor migration model, this could include comparisons of spatial moments, clustering metrics, or correlation functions of simulated labor densities with observed migration and employment data [37,56]. For the crime model, validation could involve applying hotspot detection methods to both simulated and empirical crime intensity fields, followed by comparisons of hotspot number, spatial scale, and persistence [29,58]. These pattern-based analyses would help calibrate parameters and assess the robustness of the predicted spatio-temporal structures.

A growing class of individual- and agent-based models integrates microscopic rules and experimental data, ranging from lattice-based random walks to continuous motion with chemosensory responses [59]. Multiscale methods link these descriptions to continuum models, such as those of the Keller–Segel type, thereby connecting microscopic signaling mechanisms to population-level chemotactic behavior. A deeper understanding of chemotaxis, facilitated by these modeling approaches, is expected to help address many open problems in processes driven by chemotaxis [1].

5. Conclusions

The chemotaxis-type governing Equation (1b) can be applied to simulate spatio-temporal patterns similar to the experimentally observed patterns, as well as to study the dynamics of various chemotactic-like systems such as a bacterial self-organization (Figures 2a,d and 3a), a capital-induced labor force migration (Figures 2b,e and 3b) and a criminal hotspots formation (Figures 2c,f and 3c). The specificity of the population is mathematically expressed by specific functions (6)–(10) of the chemotactic sensitivity h, the population growth and death rate f, and the production g_p and degradation g_d rates of the attractant.

By examining three established chemotaxis models within a unified framework, this study highlights how different modeling assumptions give rise to distinct qualitative behaviors. The contribution lies in comparative insight that supports mathematical understanding and model application.

The comparative analysis shows that chemotaxis-type models, though rarely applied systematically to socio-economic systems, provide a unified mathematical framework for aggregation in bacterial and human populations, with qualitative differences governed primarily by the form of their nonlinear interaction terms.

A unit disk (circle) is a suitable domain for studying the spatial dynamics of various chemotactic-like systems. The dynamics near the disk edge can be qualitatively studied using a 1D model defined on an interval Ω_1 corresponding to the disk circumference. Applying the 2D model to the disk Ω_2 results in a more accurate overview of the system and provides additional insights into the spatial dynamics of the population.

The spatial distribution of clusters of individuals in the population domain depends on the type of boundary conditions as well as on the form of specific functions (6)–(10). The

disk edge is an attractive site for the accumulation of various chemotactic populations (Figures 3 and 4a). The results of numerical simulations, together with a relationship (12) between the dimensional and dimensionless model parameters, can be used to estimate dimensional parameters such as the diffusion coefficients.

Although a human population moves over a much larger domain than biological cells, the movement toward an attractant in the human population can be considered similar to the chemotactic movement in a bacterial population, except for the significant difference in scale. The chemotaxis-type model can be used to study different behaviors of bacterial and human populations, typical of nomadic and sedentary populations (Figures 2 and 3).

In this study, we demonstrated that Keller–Segel type models can provide a reasonable approximation of certain socio-economic processes in large human populations, such as those found in major cities, countries, or continents. However, these models are not suitable for describing small groups of individuals, where unique personal traits and stochastic effects play a dominant role and cannot be captured by continuum approximations.

The results presented in this work are restricted to the case of zero-flux conditions in 2D modeling and periodic conditions in 1D modeling applied to the boundaries of the population domain. Since boundary conditions can affect the formation of spatio-temporal patterns [32,39], a more detailed investigation of their role in pattern formation remains the subject of future research. Another limitation of this study is the lack of detailed external validation using independent empirical datasets for the human migration and crime models, which restricts the generalizability of the findings. Addressing this limitation through validation against real-world data will be a key focus of future work. Finally, the present model assumes spatially homogeneous diffusion coefficients; extending the framework to incorporate spatially heterogeneous diffusion represents a further natural and biologically motivated avenue for future research [8,11,24,34,36].

To better simulate population patterns that match experimentally observed data and to improve the estimation of dimensional parameters, additional forms of the forcing functions, used for population growth and death, the chemotactic sensitivity, and the production and degradation of the attractant, should be applied and studied [3,11,14,24,35].

Author Contributions: Conceptualization, R.B. and R.Š.; methodology, R.B. and R.Š.; software, R.B. and B.D.; validation, R.B., R.Š. and B.D.; formal analysis, R.B., R.Š. and B.D.; investigation, R.B. and R.Š.; resources, R.B. and R.Š.; data curation, R.B. and R.Š.; writing—original draft preparation, R.B.; writing—review and editing, R.B., R.Š. and B.D.; visualization, R.B. and R.Š.; and supervision, R.B. All authors have read and agreed to the published version of the manuscript.

Funding: This research received no external funding.

Data Availability Statement: The original contributions presented in this study are included in the article. Further inquiries can be directed to the corresponding author.

Conflicts of Interest: The authors declare no conflicts of interest.

References

1. Simmchen, J.; Gordon, D.; MacKenzie, J.; Pagonabarraga, I.; Roggatz, C.; Endres, R.; Xiao, Z.; Friedrich, B.; Qiu, T.; Painter, K.; et al. Perspective on interdisciplinary approaches on chemotaxis. *Angew. Chem. Int. Ed.* **2025**, *64*, e202504790. [CrossRef]
2. Eisenbach, M. *Chemotaxis*; Imperial College Press: London, UK, 2004.
3. Painter, K. Mathematical models for chemotaxis and their applications in self-organization phenomena. *J. Theor. Biol.* **2019**, *481*, 162–182. [CrossRef] [PubMed]
4. Budrene, E.; Berg, H. Dynamics of formation of symmetrical patterns by chemotactic bacteria. *Nature* **1995**, *376*, 49–53. [CrossRef]
5. Hillen, T.; Painter, K. A user's guide to PDE models for chemotaxis. *J. Math. Biol.* **2009**, *58*, 183–217. [CrossRef] [PubMed]
6. Tyson, R.; Stern, L.; LeVeque, R. Fractional step methods applied to a chemotaxis model. *J. Math. Biol.* **2000**, *41*, 455–475. [CrossRef]

7. Tuval, I.; Cisneros, L.; Dombrowski, C.; Wolgemuth, C.W.; Kessler, J.; Goldstein, R.E. Bacterial swimming and oxygen transport near contact lines. *Proc. Natl. Acad. Sci. USA* **2005**, *102*, 2277–2282. [CrossRef]
8. Coppens, B.; Belpaire, T.; Pešek, J.; Steenackers, H.; Ramon, H.; Smeets, B. Anomalous diffusion of nanoparticles in the spatially heterogeneous biofilm environment. *iScience* **2023**, *26*, 106861. [CrossRef] [PubMed]
9. Keller, E.; Segel, L. Model for chemotaxis. *J. Theor. Biol.* **1971**, *30*, 225–234. [CrossRef]
10. Chertock, A.; Fellner, K.; Kurganov, A.; Lorz, A.; Markowich, P.A. Sinking, merging and stationary plumes in a coupled chemotaxis-fluid model: A high-resolution numerical approach. *J. Fluid Mech.* **2012**, *694*, 155–190. [CrossRef]
11. Bellomo, N.; Outada, N.; Soler, J.; Tao, Y.; Winkler, M. Chemotaxis and cross-diffusion models in complex environments: Models and analytic problems toward a multiscale vision. *Math. Models Methods Appl. Sci.* **2022**, *32*, 713–792. [CrossRef]
12. Neto, J.; Claeyssen, J.; Pôrto Júnior, S. Returns to scale in a spatial Solow-Swan economic growth model. *Phys. A Stat. Mech. Appl.* **2019**, *533*, 122055. [CrossRef]
13. Li, B.; Li, Y. On a chemotaxis-type Solow-Swan model for economic growth with capital-induced labor migration. *J. Math. Anal. Appl.* **2022**, *511*, 126080.
14. Neto, J.; de Almeida Konzen, P.; Claeyssen, J. A Model of Economic Growth in Two Spatial Dimensions. *Proceeding Ser. Braz. Soc. Comput. Appl. Math.* **2023**, *10*, 010011. [CrossRef]
15. Short, M.; D'Orsogna, M.; Pasour, V.; Tita, G.; Brantingham, P.; Bertozzi, A.; Chayes, L. A statistical model of criminal behavior. *Math. Models Methods Appl. Sci.* **2008**, *18*, 1249–1267.
16. Short, M.; Bertozzi, A.; Brantingham, P. Nonlinear Patterns in Urban Crime: Hotspots, Bifurcations, and Suppression. *SIAM J. Math. Anal.* **2010**, *9*, 462–483. [CrossRef]
17. Li, B.; Wang, Z.; Xie, L. Regularization effect of the mixed-type damping in a higher-dimensional logarithmic Keller-Segel system related to crime modeling. *Math. Biosci. Eng.* **2023**, *20*, 4532–4559. [CrossRef]
18. Rodriguez, N.; Bertozzi, A. Local existence and uniqueness of solutions to a PDE model for criminal behavior. *Math. Models Methods Appl. Sci.* **2010**, *20*, 1425–1457. [CrossRef]
19. Li, B.; Xie, L. Smoothness effects of a quadratic damping term of mixed type on a chemotaxis-type system modeling propagation of urban crime. *Nonlinear Anal. Real World Appl.* **2023**, *73*, 103912. [CrossRef]
20. Kurt, H.; Shen, W. Finite-Time Blow-Up Prevention by Logistic Source in Parabolic-Elliptic Chemotaxis Models with Singular Sensitivity in Any Dimensional Setting. *SIAM J. Math. Anal.* **2021**, *53*, 973–1003. [CrossRef]
21. Zhao, Y.; Xie, L. Global classical solvability and asymptotic behaviors of a parabolic-elliptic Chemotaxis-type system modeling crime activities. *J. Math. Anal. Appl.* **2024**, *532*, 127909. [CrossRef]
22. Tabata, M.; Eshima, N.; Takagi, I. A geometrical similarity between migration of human population and diffusion of biological particles. *Nonlinear Anal. Real World Appl.* **2006**, *7*, 872–894. [CrossRef]
23. Tabata, M.; Eshima, N.; Takagi, I. A mathematical modeling approach to the formation of urban and rural areas: Convergence of global solutions of the mixed problem for the master equation in sociodynamics. *Nonlinear Anal. Real World Appl.* **2011**, *12*, 3261–3293. [CrossRef]
24. Balcı, M. Distributed order model of labor migration. *Int. J. Nonlinear Sci. Numer. Simul.* **2023**, *24*, 2497–2512.
25. Šimkus, R.; Baronas, R. Metabolic self-organization of bioluminescent *Escherichia coli*. *Luminescence* **2011**, *26*, 716–721. [CrossRef]
26. Baronas, R.; Ledas, Ž.; Šimkus, R. Computational modeling of self-organization in a liquid phase bacterial bioluminescent biosensor. In Proceedings of the 6th European Congress on Computational Methods in Applied Sciences and Engineering (ECCOMAS 2012), Vienna, Austria, 10–14 September 2012; p. Paper ID: 4815.
27. Baronas, R.; Ledas, Ž.; Šimkus, R. Computational modeling of the bacterial self-organization in a rounded container: The effect of dimensionality. *Nonlinear Anal. Model. Control* **2015**, *20*, 603–620. [CrossRef]
28. Šimkus, R.; Baronas, R.; Ledas, Ž. A multi-cellular network of metabolically active *E. coli* as a weak gel of living Janus particles. *Soft Matter* **2013**, *9*, 4489–4500. [CrossRef]
29. Gu, Y.; Wang, Q.; Yi, G. Stationary patterns and their selection mechanism of urban crime models with heterogeneous near-repeat victimization effect. *Eur. J. Appl. Math.* **2017**, *28*, 141–178. [CrossRef]
30. Samarskii, A. *The Theory of Difference Schemes*; Marcel Dekker: New York, NY, USA; Basel, Switzerland, 2001.
31. Maini, P.; Myerscough, M.; Winters, K.; Murray, J. Bifurcating spatially heterogeneous solutions in a chemotaxis model for biological pattern generation. *Bull. Math. Biol.* **1991**, *53*, 701–719. [PubMed]
32. Painter, K.; Hillen, T. Spatio-temporal chaos in a chemotactic model. *Phys. D Nonlinear Phenom.* **2011**, *240*, 363–375. [CrossRef]
33. Qiu, Z.; Li, B. Eventual smoothness of generalized solutions to a singular chemotaxis system for urban crime in space dimension 2. *Electron. Res. Arch.* **2023**, *31*, 3218–3244. [CrossRef]
34. Cherstvy, A.; Metzler, R. Ergodicity breaking and particle spreading in noisy heterogeneous diffusion processes. *J. Chem. Phys.* **2015**, *142*, 144105. [CrossRef] [PubMed]
35. Ballestra, L. Modeling economic growth with spatial migration: A stability analysis of the long-run equilibrium based on semigroup theory. *J. Math. Anal. Appl.* **2024**, *531*, 127794. [CrossRef]

36. Rodriguez, N.; Winkler, M. Relaxation by nonlinear diffusion enhancement in a two-dimensional cross-diffusion model for urban crime propagation. *Math. Models Methods Appl. Sci.* **2020**, *30*, 2105–2137. [CrossRef]
37. Balcı, M. Time fractional capital-induced labor migration model. *Phys. A Stat. Mech. Appl.* **2017**, *477*, 91–98. [CrossRef]
38. Fu, S.; Liu, J. Spatial pattern formation in the Keller-Segel model with a logistic source. *Comput. Math. Appl.* **2013**, *66*, 403–417. [CrossRef]
39. Murray, J. *Mathematical Biology: II. Spatial Models and Biomedical Applications*, 3rd ed.; Springer: Berlin, Germany, 2003.
40. Pitcher, A. Adding police to a mathematical model of burglary. *Eur. J. Appl. Math.* **2010**, *21*, 401–419. [CrossRef]
41. Ispolatov, J.; Doebeli, M. Diversification along environmental gradients in spatially structured populations. *Evol. Ecol. Res.* **2004**, *11*, 295–304.
42. Tisbury, A.; Needham, D.; Tzella, A. The evolution of traveling waves in a KPP reaction-diffusion model with cut-off reaction rate. I. Permanent form traveling waves. *Stud. Appl. Math.* **2021**, *146*, 301–329.
43. Myerscough, M.; Maini, P.; Painter, K. Pattern formation in a generalized chemotactic model. *Bull. Math. Biol.* **1998**, *60*, 1–26. [CrossRef] [PubMed]
44. Čiegis, R.; Bugajev, A. Numerical approximation of one model of bacterial self-organization. *Nonlinear Anal. Model. Control* **2012**, *17*, 253–270. [CrossRef]
45. Heihoff, F. Generalized solutions for a system of partial differential equations arising from urban crime modeling with a logistic source term. *Z. Angew. Math. Phys.* **2020**, *71*, 80. [CrossRef]
46. Ureña, N.; Vargas, A. On the numerical solution to a Solow model with spatial diffusion and technology-induced capital mobility. *Eng. Anal. Bound. Elem.* **2023**, *157*, 541–552. [CrossRef]
47. Šimkus, R.; Meškienė, R.; Aučynaitė, A.; Ledas, Ž.; Baronas, R.; Meškys, R. Phoretic interactions and oscillationsin active suspensions of growing *Escherichia coli*. *R. Soc. Open Sci.* **2018**, *5*, 180008.
48. Lai, M.C. A note on finite difference discretizations for Poisson equation on a disk. *Numer. Methods Partial. Differ. Equ.* **2001**, *17*, 199–203.
49. Knoll, P.; Mirzaei, S. Scientific computing with Java. *Comput. Appl. Eng. Educ.* **2010**, *18*, 495–501. [CrossRef]
50. Moberly, J.; Bernards, M.; Waynant, K. Key features and updates for Origin 2018. *J. Cheminform.* **2018**, *10*, 5.
51. Šimkus, R.; Kirejev, V.; Meškienė, R.; Meškys, R. Torus generated by *Escherichia coli*. *Exp. Fluids* **2009**, *46*, 365–369. [CrossRef]
52. Brenner, M.; Levitov, L.; Budrene, E. Physical mechanisms for chemotactic pattern formation by bacteria. *Biophys. J.* **1998**, *74*, 1677–1693. [CrossRef] [PubMed]
53. Berg, H.; Turner, L. Chemotaxis of bacteria in glass capillary arrays. *Biophys. J.* **1990**, *58*, 919–930. [CrossRef]
54. Perry, N. Experimental validation of a critical domain size in reaction-diffusion systems with *Escherichia coli* populations. *J. R. Soc. Interface* **2005**, *2*, 379–387.
55. Czaika, M.; de Haas, H. The Globalization of Migration: Has the world really become more migratory? *Int. Migr. Rev.* **2015**, *48*, 283–323. [CrossRef]
56. Stillwell, J.; Bell, M.; Ueffing, P.; Daras, K.; Charles-Edwards, E.; Kupiszewski, M.; Kupiszewska, D. Internal migration around the world: Comparing distance travelled and its frictional effect. *Environ. Plan. A* **2016**, *48*, 1657–1675. [CrossRef]
57. Kolter, R.; Greenberg, E. The superficial life of microbes. *Nature* **2006**, *441*, 300–302. [CrossRef] [PubMed]
58. D'Orsogna, M.; Perc, M. Statistical physics of crime: A review. *Phys. Life Rev.* **2015**, *12*, 1–21. [CrossRef] [PubMed]
59. Railsback, S.; Grimm, V. *Agent-Based and Individual-Based Modeling: A Practical Introduction*; Princeton University Press: Princeton, NJ, USA, 2019.